Continuous-wave lasing in an organic-inorganic lead halide perovskite semiconductor

Yufei Jia[1], Ross A. Kerner[2], Alex J. Grede[1], Barry P. Rand[2], Noel C. Giebink[1†]

[1]*Department of Electrical Engineering, The Pennsylvania State University, University Park, PA 16802,USA*

[2]*Department of Electrical Engineering and Andlinger Center for Energy and the Environment, Princeton University, Princeton, NJ 08544,USA*

[†]email: ncg2@psu.edu

Abstract

Hybrid organic-inorganic perovskites have emerged as promising gain media for tunable, solution-processed semiconductor lasers; however, continuous-wave (CW) operation has not been achieved to date. Here, we demonstrate that optically-pumped CW lasing can be sustained above threshold excitation intensities of ~17 kW/cm^2 for over an hour in methylammonium lead iodide ($MAPbI_3$) distributed feedback lasers that are maintained below the $MAPbI_3$ tetragonal-to-orthorhombic phase transition temperature, $T \sim 160$ K. In contrast to the lasing death phenomenon that occurs for pure tetragonal phase $MAPbI_3$ at $T > 160$ K, we find that CW gain becomes possible at $T \sim 100$ K from tetragonal phase inclusions that are photogenerated by the pump within the normally-existing, larger bandgap orthorhombic host matrix. In this mixed phase system, the tetragonal inclusions function as carrier recombination sinks that reduce the transparency threshold, in loose analogy to inorganic semiconductor quantum wells, and may serve as a model for engineering improved perovskite gain media.

Keywords: lead halide perovskite, continuous wave, laser, distributed feedback

After nearly twenty years of intense research, electrically-pumped lasing remains an elusive grand challenge for the organic and thin film electronics community and would mark a technological advance with application potential rivaling that of organic light emitting diodes.[1-3] Recently, hybrid organic-inorganic perovskite semiconductors − the same materials that have ignited the photovoltaics world − have also emerged as efficient light emitters with attractive gain characteristics, renewing hope for a tunable, solution-processed laser diode and setting up a worldwide race to achieve this goal.[3-5]

Continuous-wave (CW) optically-pumped lasing is widely believed to be a key stepping-stone on the path to an electrically-pumped laser diode.[1-3] It has never been accomplished with organic semiconductors[6-8] and was only recently reported for colloidal quantum dots.[9-11] Recent attempts to achieve CW distributed feedback (DFB) lasing from methylammonium lead iodide ($MAPbI_3$) perovskite in its tetragonal phase (which exists at temperatures $T > 160$ K) found that lasing ceases within tens of nanoseconds following the pump turn-on.[12] The origin of this lasing death phenomenon presently remains unclear, although thermal runaway and Auger loss have been ruled out.[12]

Here, we report an interesting twist: true CW lasing is possible from the *same* perovskite semiconductor, but at temperatures below its tetragonal-to-orthorhombic phase transition ($T = 160$ K). In this case, gain originates from small *tetragonal* phase volumes that are photogenerated by the pump. At a substrate temperature of roughly 100 K, our second-order $MAPbI_3$ DFB lasers achieve threshold at a pump intensity of $I_{\mathrm{th}} \sim 17$ kW/cm^2 and sustain CW lasing with a clear output beam for over one hour. We propose that the photogenerated tetragonal phase inclusions may act as charge carrier sinks within the larger bandgap orthorhombic phase host matrix, enhancing the population inversion in analogous fashion to host/guest organic

semiconductor gain media and inorganic quantum wells.[13,14] These results point toward a general strategy to design perovskite gain media for CW lasing and represent a key step toward the ultimate goal of a perovskite laser diode.

Figure 1 explores the amplified spontaneous emission (ASE) gain dynamics of a 120 nm thick $MAPbI_3$ film deposited on a sapphire substrate using an InGaN pump diode ($\lambda_P = 445$ nm, intensity $I_P = 37.5$ kW/cm^2, 920 ns long pulses at 100 Hz repetition rate) and a streak camera. In Fig. 1a at a substrate temperature, $T = 169$ K, tetragonal-phase ASE is observed immediately following the pump turn-on but ceases within roughly 100 ns, giving way to incoherent photoluminescence through the end of the pump pulse. This is consistent with the lasing death phenomenon identified in Ref. [12]. The situation is much different in Fig. 1b when the substrate is held well below the phase transition temperature at $T = 106$ K. There, ASE is initially observed from the orthorhombic phase (peaking at $\lambda \sim 750$ nm) but quickly transitions into tetragonal phase ASE (peaking at $\lambda \sim 790$ nm) that is sustained until the end of the pump pulse; details supporting the assignment of ASE in each case are provided in Supplementary Fig. S1.

Inspired by the long-lived ASE, we fabricated a second-order DFB laser by depositing a similar, ~120 nm thick $MAPbI_3$ film onto a $\Lambda = 385$ nm period grating etched into a thin alumina layer on a high thermal conductivity sapphire substrate. This particular structure is designed to support the fundamental transverse electric (TE_0) mode with a modal effective index that satisfies the Bragg feedback condition at the peak of the tetragonal phase ASE spectrum. Figure 2a shows a cross-sectional scanning electron micrograph of a typical sample, highlighting the low surface roughness of the $MAPbI_3$ film enabled by our solvent exchange deposition process.[15]

Figure 2b shows the input-output characteristic obtained for the laser structure under CW excitation by the InGaN pump diode at a substrate temperature of $T = 102$ K. There, we observe a clear threshold at $I_{\mathrm{P}} = 17 \pm 1$ kW/cm^2 and a TE-polarized laser line above threshold (Fig. 2b, inset) that systematically red-shifts with further increase in the pump intensity as shown in Fig. 2c. Figure 2d shows a photograph of the surface-emitted CW beam profile projected on a card located ~6 cm away. The fan-like pattern is indicative of a second order DFB laser dominated by index coupling, though we note that in other samples with more deeply-etched gratings, a double-lobed fan pattern indicative of gain/loss coupling was also observed.[16,17] Taken together, these data unequivocally demonstrate lasing.

Figure 3a and 3b confirm CW lasing over timescales ranging from microseconds (Fig. 3a) to minutes (Fig. 3b). Consistent with the ASE behavior in Fig. 1b, there is a few hundred nanosecond delay, Δt_D, between the pump turn-on at time zero and the onset of laser emission in Fig. 3a that is usually followed by a curious 'wiggle' in the emission wavelength. In general, Δt_D decreases with increasing pump intensity and/or increasing substrate temperature and the emission line wiggle can even become a damped oscillation as shown in Supplementary Fig. S2. At long time scales, the laser line exhibits a slow blue-shift and reduces in intensity over the course of ~10 minutes (see Fig. 3b), though in some of the samples we tested, lasing could be sustained for more than one hour (see Fig. 3c). A video of the CW laser operation is provided in the Supplementary Material.

It is important to point out that, while CW lasing is robust and repeatable for a given sample set over the course of many months of testing, the details change from day to day and depend on the history of a particular sample. For example, we observe hysteresis in the laser threshold (roughly $\pm 25\%$ variation) and emission wavelength (roughly ± 3 nm) between heating

and cooling cycles, similar to previous temperature-dependent photoluminescence measurements.[18,19] Additionally, over the course of several heating and cooling cycles, our samples exhibit slow increases in their threshold (see Supplementary Fig. S3) and the form of their sub-μs wavelength variation changes (see, e.g. the difference in the wiggle between Fig. 3a and Supplementary Fig. S2). This is likely related to morphological and crystal texture changes that occur upon heating and cooling as discussed previously by Osherov *et al*.[19]

Although the CW gain and lasing above originate from the tetragonal phase (emission at $\lambda \sim 785$ nm), Fig. 4 suggests that the majority of the $MAPbI_3$ film remains in the orthorhombic phase. There, the transient absorption (TA) counterpart of the emission evolution in Fig. 1b shows a bleach at the orthorhombic band edge corresponding to the short-lived orthorhombic ASE in Fig. 1b. However, the TA data do not show any tetragonal phase absorption associated with the crossover to tetragonal ASE in Fig. 1b which, based on the noise floor of the measurement and the transmission change expected for complete conversion (shown by the green line in the lower panel), limits the tetragonal phase volume fraction of the film to less than 1%.

This is consistent with the observations of Panzer *et al*.[20], who found that tetragonal phase ASE could be induced at low temperature ($T << 160$ K) in the orthorhombic phase after first illuminating with one or more high energy (~mJ/cm^2) laser pulses. These authors proposed that local heating by the laser pulse can trigger the formation of tetragonal phase inclusions that are kinetically trapped within the orthorhombic bulk. Because the tetragonal phase bandgap is lower than that of the orthorhombic phase, these sites serve as efficient carrier sinks and become the dominant recombination pathway. This is closely related to the orthorhombic/tetragonal phase coexistence that naturally occurs (even without photo-triggering) in $MAPbI_3$ over a finite

temperature window (the range of which depends on factors such as processing route and grain size) in the vicinity of the nominal $T = 160$ K phase transition temperature.[18,19,21] Based on the temperature-dependent photoluminescence in Supplementary Fig. S4, the natural phase coexistence temperature range of our films is approximately $120 < T < 160$ K.

In the present context, the picture of CW gain that emerges is the following. Upon illuminating a low temperature orthorhombic $MAPbI_3$ film with a sufficiently intense pump, the associated heat dissipation triggers certain locations (likely predisposed by defects or grain boundaries[22]) to transition into the tetragonal phase. Crucially, because photogenerated carriers rapidly accumulate within these tetragonal energetic wells,[18,23] their population inversion is increased relative to that of a pure tetragonal phase film under the same excitation conditions, in much the same manner as traditional inorganic semiconductor quantum well and organic semiconductor host/guest gain media.[13,14] The possibility of exploiting this mixed phase carrier concentration mechanism for CW gain in $MAPbI_3$ was actually noted previously by Wehrenfennig *et al*.[18] and Neutzner *et al*.[23], though it remains unclear whether other aspects associated with the low temperature mixed phase system are also important as discussed below.

At the $T \geq 80$ K substrate temperatures used in our experiments, the tetragonal regions are short lived. When the pump is turned off, they begin to revert back to the orthorhombic phase on a microsecond timescale (see Supplementary Fig. S5), though we note that the reversion rate is strongly temperature-dependent since they are reported to be metastable at $T = 5$ K.[20] It therefore seems likely that, under our CW lasing conditions, the tetragonal inclusions exist in a dynamic equilibrium, with their size determined by a balance between pump-induced heating (which causes them to grow) and heat extraction into the substrate (which causes them to shrink). This is consistent with thermal modeling in Supplementary Fig. S6, which indicates that the

equilibrium temperature of CW lasing $MAPbI_3$ falls within the 120 − 160 K mixed-phase temperature range established from photoluminescence in Supplementary Fig. S4.

This situation may explain the red-shift in lasing wavelength with increasing pump power shown in Fig. 2c, which is notable since pure tetragonal phase emission and lasing normally blue-shifts upon heating (due to the increasing pump power).[12] In the mixed phase, however, the tetragonal emission exhibits an anomalous red-shift with increasing temperature[19,21] (see Supplementary Fig. S4) that would explain the observed shift in lasing wavelength. As argued previously,[18,22] this may result from strain imposed by the orthorhombic bulk, which causes the bandgap of the tetragonal inclusions to increase. The relative strain lessens with increasing temperature since the growing tetragonal phase displaces more of the confining orthorhombic phase, which leads to the anomalous red-shift in emission and in turn to the increase in lasing wavelength with pump power. Such a strain-induced bandgap shift with tetragonal phase volume fraction may also underlie the early time instability in lasing wavelength (e.g. in Fig. 3a) as the size of the inclusions evolves rapidly upon pump turn-on.

Moving forward, it will be important to uncover the physical origin of $MAPbI_3$ lasing death at temperatures above 160 K and, in particular, why CW gain is possible from tetragonal phase inclusions but not from the tetragonal phase bulk. While the mixed phase system should reduce the threshold carrier density required for transparency, it is not expected to increase the modal gain of the $MAPbI_3$ film since the enhanced population inversion in tetragonal inclusions is equally offset by their reduced volume fraction (and thus overlap with the lasing mode).[13] Based on the fact that a mere ~70 K difference in substrate temperature constitutes the difference between CW gain and lasing death in the same film despite a *lower* gain threshold in the pure tetragonal phase (see Supplementary Fig. S1), it seems likely that there is more to the story than

just the carrier concentration effect. For example, dielectric screening in the inclusions may be affected by the large dielectric constant reduction in the surrounding orthorhombic phase and its associated restriction of the methylammonium cation rotational freedom.[24,25] Alternatively, strain itself may be key, as recent work has uncovered a significant increase in $MAPbI_3$ radiative rate (and thus stimulated emission cross-section) under hydrostatic pressure as it becomes increasingly direct bandgap.[26]

In summary, we have demonstrated second-order $MAPbI_3$ distributed feedback lasers that operate CW for over an hour above optical pumping thresholds of ~17 kW/cm^2 and at temperatures below the tetragonal-to-orthorhombic phase transition ($T < 160$ K). Continuous gain originates from tetragonal phase inclusions that are photogenerated by the pump within the bulk orthorhombic host matrix on a sub-microsecond time scale. While more work is required to fully understand why this mixed phase arrangement avoids the lasing death phenomenon that occurs for pure tetragonal phase $MAPbI_3$ at $T > 160$ K, our results suggest that engineering perovskite gain media to mimic the same host/guest energy level scheme[27-29] may be a useful strategy moving forward in pursuit of an electrically-pumped laser diode.

Methods

Fabrication. Distributed feedback gratings were created by first depositing an 80 nm thick Al_2O_3 layer onto a sapphire substrate, followed by a 100 nm thick layer of S1805 photoresist which was patterned using interference lithography as described previously. The gratings were developed and hard-baked at 150 °C for 5 minutes followed by a wet etch in 85% H_2PO_4 for 50 s at 68 °C to transfer the pattern into the underlying Al_2O_3. Methylammonium iodide (MAI) was synthesized by mixing aqueous HI (Aldrich) with equimolar methylamine (ethanol solution, Aldrich) for 2 h at 0 °C. The MAI was then purified by recrystallization from hot

isopropanol:toluene (~1:4) mixture. The $MAPbI_3$ active layer was subsequently deposited onto the gratings by spin-coating a 0.65 M solution of stoichiometric MAI/PbI_2 (Alfa) in DMF at ~5200 rpm. The solution was filtered with a 200 nm PTFE filter prior to spinning. To obtain a smooth film of high optical quality, a solvent exchange was performed by pipetting ~0.5 mL of toluene at 4 s after starting the spinning, which results in the formation of nano-crystallites and approximately 4 nm RMS roughness. The films were dried for approximately 5 minutes on a hot plate and stored in the dark in N_2 during the several months it took to complete the laser characterization.

Characterization. All measurements were carried out under vacuum in a continuous-flow liquid nitrogen cryostat. Temperature was recorded from a Si temperature diode mounted directly on the substrate surface with thermal grease, approximately 10 mm from the pump spot. Samples were pumped with a 3.5 W blue Nichia NDB7K75 InGaN laser diode driven by a PicoLAS LDP-V 03-100 pulsed or LDP-CW 18-05 CW current source. A planoconvex lens was used to focus light directly from the output facet to a full-width half-maximum 120×30 μm^2 stripe on the sample, as measured using a CMOS camera placed in the sample plane. Under CW lasing excitation, the substrate temperature measured by the Si diode typically increased by ~10 K over its value in the dark due to heat dissipation by the pump; this is consistent with thermal modeling presented in Supplementary Fig. S6. All of the substrate temperatures reported here reference the illuminated condition.

Time-resolved emission was collected and focused using a pair of off-axis parabaloidal reflectors into a Hamamatsu C10910 streak camera with a 1/8 m monochromator and a spectral resolution limit of $\Delta\lambda = 0.5$ nm. CW emission was measured using a CCD-coupled spectrograph with $\Delta\lambda = 0.05$ nm spectral resolution. The far-field emission profile of the DFB lasers was

imaged on a white card at a distance of approximately 6 cm using a CMOS camera with a 600 nm long-pass filter to reject stray pump light.

Transient absorption experiments were conducted with a Fianium WhiteLase SC400 super-continuum probe beam arranged within the experimental setup shown in Supplementary Fig. S7. The ~6 ps pulse width probe light was passed through a 1/8 m monochromator and focused using a pair of cylindrical lenses to a similar size spot overlapping the diode laser pump. The super-continuum source was pulse-picked to a repetition rate of 500 kHz and used in conjunction with a frequency divider and a digital delay unit to trigger the diode laser pump at 125 kHz so that one out of every four probe pulses overlapped near the pump in time. The change in probe transmission, ΔT, induced by the pump at varying delays was then detected synchronously with a Si photodiode and a lock-in amplifier.

References

1 Samuel, I. D. W. & Turnbull, G. A. Organic semiconductor lasers. *Chem. Rev.* **107**, 1272-1295, (2007).

2 Chénais, S. & Forget, S. Recent advances in solid-state organic lasers. *Polymer Internat.* **61**, 390-406, (2012).

3 Sutherland, B. R. & Sargent, E. H. Perovskite photonic sources. *Nat. Photon.* **10**, 295-302, (2016).

4 Veldhuis, S. A., Boix, P. P., Yantara, N., Li, M., Sum, T. C., Mathews, N. & Mhaisalkar, S. G. Perovskite materials for light-emitting diodes and lasers. *Adv. Mater.* **28**, 6804-6834, (2016).

5 Xing, G., Mathews, N., Lim, S. S., Yantara, N., Liu, X., Sabba, D., Grätzel, M., Mhaisalkar, S. & Sum, T. C. Low-temperature solution-processed wavelength-tunable perovskites for lasing. *Nat. Mater.* **13**, 476-480, (2014).

6 Giebink, N. C. & Forrest, S. R. Temporal response of optically pumped organic semiconductor lasers and its implication for reaching threshold under electrical excitation. *Phys. Rev. B* **79**, 073302, (2009).

7 Zhang, Y. & Forrest, S. R. Existence of continuous-wave threshold for organic semiconductor lasers. *Phys. Rev. B* **84**, 241301, (2011).

8 Sandanayaka, A. S. D., Matsushima, T., Bencheikh, F., Yoshida, K., Inoue, M., Fujihara, T., Goushi, K., Ribierre, J.-C. & Adachi, C. Toward continuous-wave operation of organic semiconductor lasers. *Sci. Adv.* **3**, e1602570, (2017).

9 Fan, F., Voznyy, O., Sabatini, R. P., Bicanic, K. T., Adachi, M. M., McBride, J. R., Reid, K. R., Park, Y.-S., Li, X., Jain, A., Quintero-Bermudez, R., Saravanapavanantham, M., Liu, M., Korkusinski, M., Hawrylak, P., Klimov, V. I., Rosenthal, S. J., Hoogland, S. & Sargent, E. H. Continuous-wave lasing in colloidal quantum dot solids enabled by facet-selective epitaxy. *Nature* **544**, 75-79, (2017).

10 Grim, J. Q., Christodoulou, S., Di Stasio, F., Krahne, R., Cingolani, R., Manna, L. & Moreels, I. Continuous-wave biexciton lasing at room temperature using solution-processed quantum wells. *Nat. Nanotech.* **9**, 891-895, (2014).

11 Yang, Z., Pelton, M., Fedin, I., Talapin, D. V. & Waks, E. A room temperature continuous-wave nanolaser using colloidal quantum wells. *Nat. Comm.* **8**, 143, (2017).

12 Jia, Y., Kerner, R. A., Grede, A. J., Brigeman, A. N., Rand, B. P. & Giebink, N. C. Diode-Pumped Organo-Lead Halide Perovskite Lasing in a Metal-Clad Distributed Feedback Resonator. *Nano Lett.* **16**, 4624-4629, (2016).

13 Blood, P. *Quantum Confined Laser Devices: Optical Gain and Recombination in Semiconductors*. (Oxford University Press, 2015).

14 Kozlov, V. G., Bulovic, V., Burrows, P. E., Baldo, M., Khalfin, V. B., Parthasarathy, G., Forrest, S. R., You, Y. & Thompson, M. E. Study of lasing action based on Forster energy transfer in optically pumped organic semiconductor thin films. *J. Appl. Phys.* **84**, 4096-4108, (1998).

15 Xiao, Z., Kerner, R. A., Zhao, L., Tran, N. L., Lee, K. M., Koh, T.-W., Scholes, G. D. & Rand, B. P. Efficient perovskite light-emitting diodes featuring nanometre-sized crystallites. *Nat. Photon.* **11**, 108-108, (2017).

16 Kogelnik, H. & Shank, C. V. Coupled-wave theory of distributed feedback lasers. *J. Appl. Phys.* **43**, 2327-2335, (1972).

17 Andrew, P., Turnbull, G. A., Samuel, I. D. W. & Barnes, W. L. Photonic band structure and emission characteristics of a metal-backed polymeric distributed feedback laser. *Appl. Phys. Lett.* **81**, 954-956, (2002).

18 Wehrenfennig, C., Liu, M., Snaith, H. J., Johnston, M. B. & Herz, L. M. Charge carrier recombination channels in the low-temperature phase of organic-inorganic lead halide perovskite thin films. *APL Mater.* **2**, 081513, (2014).

19 Osherov, A., Hutter, E. M., Galkowski, K., Brenes, R., Maude, D. K., Nicholas, R. J., Plochocka, P., Bulović, V., Savenije, T. J. & Stranks, S. D. The impact of phase retention

on the structural and optoelectronic properties of metal halide perovskites. *Adv. Mater.* **28**, 10757-10763, (2016).

20 Panzer, F., Baderschneider, S., Gujar, T. P., Unger, T., Bagnich, S., Jakoby, M., Bässler, H., Hüttner, S., Köhler, J. & Moos, R. Reversible Laser-Induced Amplified Spontaneous Emission from Coexisting Tetragonal and Orthorhombic Phases in Hybrid Lead Halide Perovskites. *Adv. Opt. Mater.* **4**, 917-928, (2016).

21 Kong, W., Ye, Z., Qi, Z., Zhang, B., Wang, M., Rahimi-Iman, A. & Wu, H. Characterization of an abnormal photoluminescence behavior upon crystal-phase transition of perovskite CH 3 NH 3 PbI 3. *Phys. Chem. Chem. Phys.* **17**, 16405-16411, (2015).

22 Dobrovolsky, A., Merdasa, A., Unger, E. L., Yartsev, A. & Scheblykin, I. G. Defect-induced local variation of crystal phase transition temperature in metal-halide perovskites. *Nat. Comm.* **8**, 34, (2017).

23 Neutzner, S., Kandada, A. R. S., Lanzani, G. & Petrozza, A. A dual-phase architecture for efficient amplified spontaneous emission in lead iodide perovskites. *J. Mater. Chem. C* **4**, 4630-4633, (2016).

24 Onoda-Yamamuro, N., Matsuo, T. & Suga, H. Dielectric study of CH3NH3PbX3 (X= Cl, Br, I). *J. Phys. Chem. Sol.* **53**, 935-939, (1992).

25 Chen, T., Foley, B. J., Ipek, B., Tyagi, M., Copley, J. R. D., Brown, C. M., Choi, J. J. & Lee, S.-H. Rotational dynamics of organic cations in the CH 3 NH 3 PbI 3 perovskite. *Phys. Chem. Chem. Phys.* **17**, 31278-31286, (2015).

26 Wang, T., Daiber, B., Frost, J. M., Mann, S. A., Garnett, E. C., Walsh, A. & Ehrler, B. Indirect to direct bandgap transition in methylammonium lead halide perovskite. *Energy Environ. Sci.* **10**, 509-515, (2017).

27 Marongiu, D., Chang, X., Sarritzu, V., Sestu, N., Pau, R., Geddo Lehmann, A., Mattoni, A., Quochi, F., Saba, M., Mura, A. & Bongiovanni, G. Self-Assembled Lead Halide Perovskite Nanocrystals in a Perovskite Matrix. *ACS Energy Lett.* **2**, 769-775, (2017).

28 Byun, J., Cho, H., Wolf, C., Jang, M., Sadhanala, A., Friend, R. H., Yang, H. & Lee, T.-W. Efficient Visible Quasi-2D Perovskite Light-Emitting Diodes. *Adv. Mater.* **28**, 7515-7520, (2016).

29 Yuan, M., Quan, L. N., Comin, R., Walters, G., Sabatini, R., Voznyy, O., Hoogland, S., Zhao, Y., Beauregard, E. M., Kanjanaboos, P., Lu, Z., Kim, D. H. & Sargent, E. H. Perovskite energy funnels for efficient light-emitting diodes. *Nat. Nanotechnol.* **11**, 872-877, (2016).

Acknowledgements

This work was supported in part by the Air Force Office of Scientific Research Young Investigator Program under Award No. FA-9550-14-1-0301 and by the National Science Foundation under Grant No. DMR-1654077. R.A.K. and B.P.R. acknowledge support from a DARPA Young Faculty Award, #D15AP00093 and ONR Young Investigator Program (Award #N00014-17-1-2005).

Author Contributions

Y.J. fabricated the gratings, carried out the laser measurements, and performed the data analysis. R.A.K. developed the perovskite processing and deposition method, and A.J.G. carried out the transient absorption measurements. B.P.R. and N.C.G. supervised the work. All authors contributed in writing the manuscript.

Additional information

Supplementary information is available in the online version of the paper. Reprints and permissions information is available online at www.nature.com/reprints. Correspondence and requests for materials should be addressed to N.C.G.

Competing Interests

The authors declare no competing financial interests.

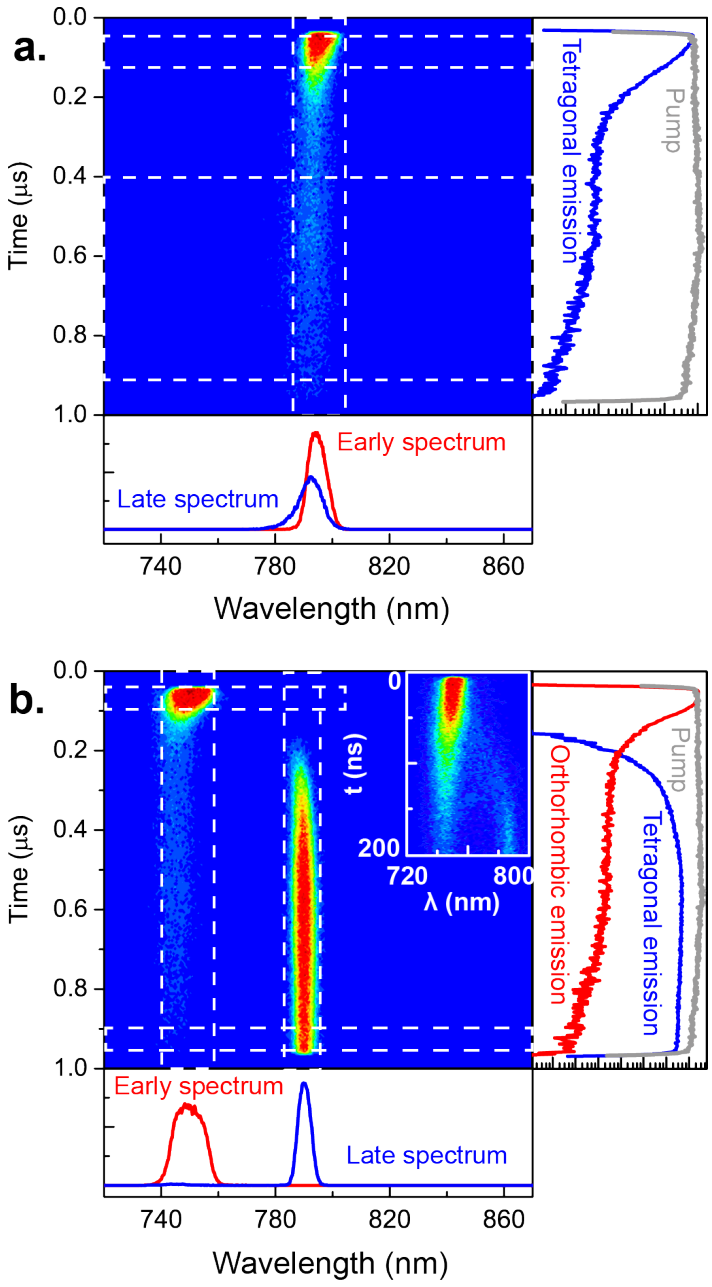

Figure 1 | Gain dynamics of $MAPbI_3$ at low temperature. a, Streak camera image showing the short-lived nature of amplified spontaneous emission (ASE) from a 120 nm thick $MAPbI_3$ film on a sapphire substrate held at $T = 169$ K in response to a 920 ns long rectangular pump pulse from an InGaN diode laser with instantaneous intensity, $I_P = 37.5$ kW/cm^2. The transient trace appended to the right-hand side of the image is the spectrally-integrated intensity within the

vertical dashed rectangle and the early and late time spectral traces at the bottom are time-integrated intensities within the horizontal dashed rectangles. **b,** Streak camera image of emission from the same film under the same pump intensity when the substrate temperature is lowered to $T = 106$ K. In this case, ASE from the orthorhombic phase of $MAPbI_3$ is observed at early times but evolves within ~200 ns (see blow-up shown in the inset) into tetragonal phase ASE that is sustained until the end of the pump pulse.

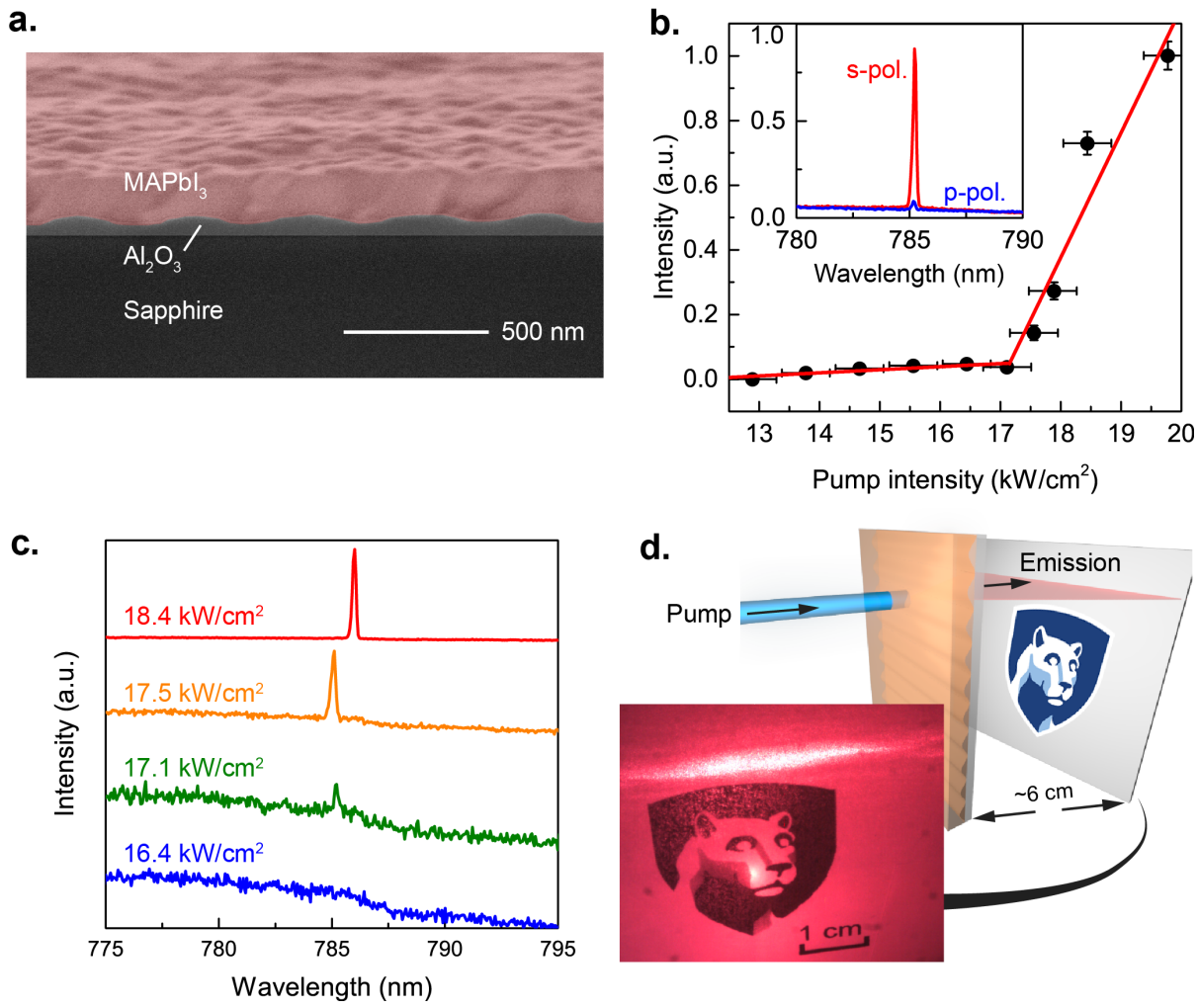

Figure 2 | CW lasing characterization. a, Cross-sectional scanning electron micrograph of the second-order distributed feedback laser architecture consisting of the $MAPbI_3$ film deposited on an 80 nm thick etched alumina grating on a sapphire substrate. Color shading has been added for clarity. **b,** Input-output characteristic of the laser under continuous excitation by a $\lambda = 445$ nm InGaN pump diode at a substrate temperature of 102 K, demonstrating a clear threshold at $I_P \sim 17$ kW/cm^2. The inset shows that the emission spectrum above threshold ($I_P = 1.21 I_{th}$) is strongly s-polarized (red), with a negligible p-polarized contribution (blue). **c,** The laser line red-shifts with increasing pump intensity and displays a full-width half-maximum linewidth, $\Delta\lambda_{FWHM} = 0.25$ nm at the highest pump intensity. **d,** Photograph of the far-field spatial profile of the laser

beam projected onto a white card as depicted in the diagram. The image was recorded by a CMOS camera using a 600 nm long-pass filter to reject stray pump light.

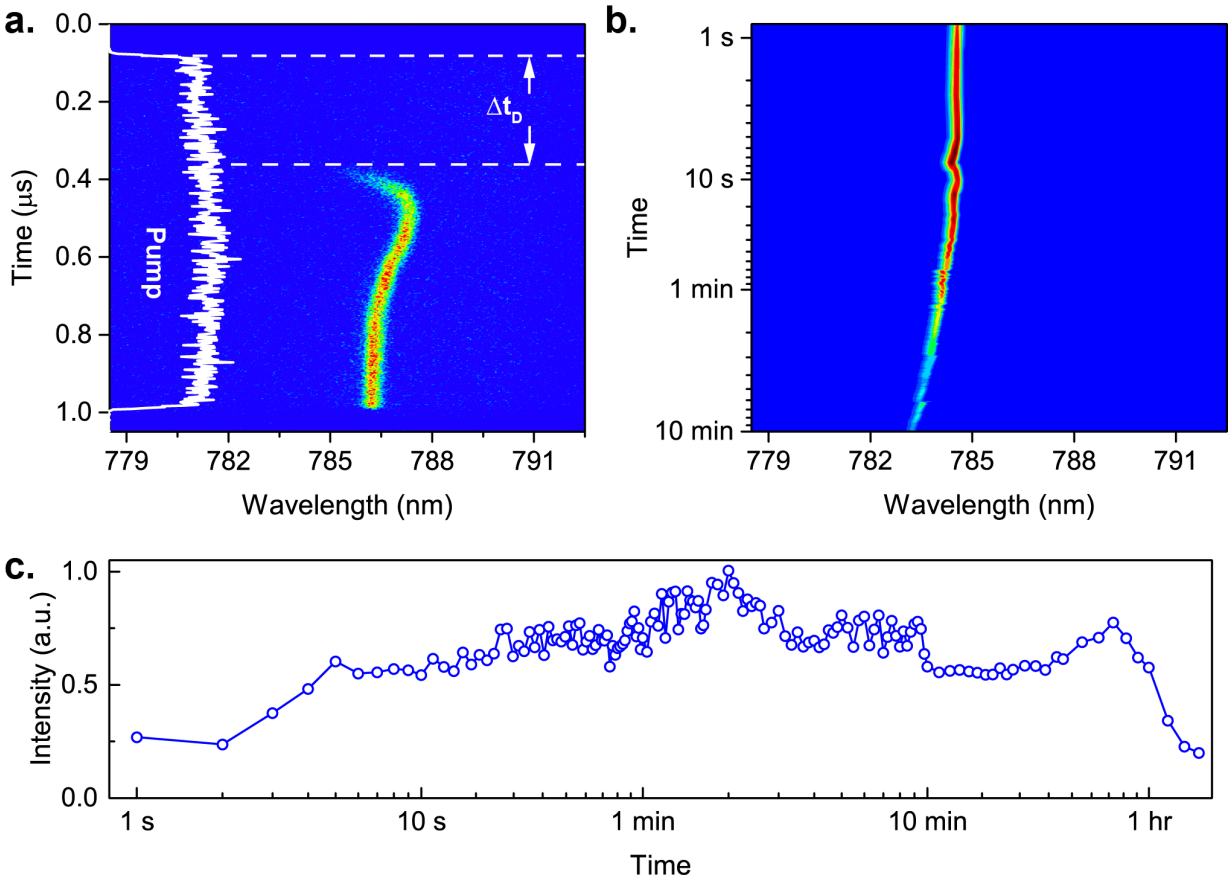

Figure 3 | CW lasing dynamics. a, Streak camera image of the laser emission observed within the first microsecond following turn-on of the pump (white trace). The pump intensity is $I_{\mathrm{P}} = 26.4\ \mathrm{kW/cm^2} = 1.55 I_{\mathrm{th}}$. **b,** Composite image obtained by collecting individual steady-state spectra (integrated over 0.1 s) over a 10 minute time period at the same pump intensity. The data in **a** and **b** are obtained from different samples on different days and therefore differences in emission wavelength between them should not be interpreted chronologically. **c,** CW laser emission intensity recorded from a single excitation spot over more than one hour.

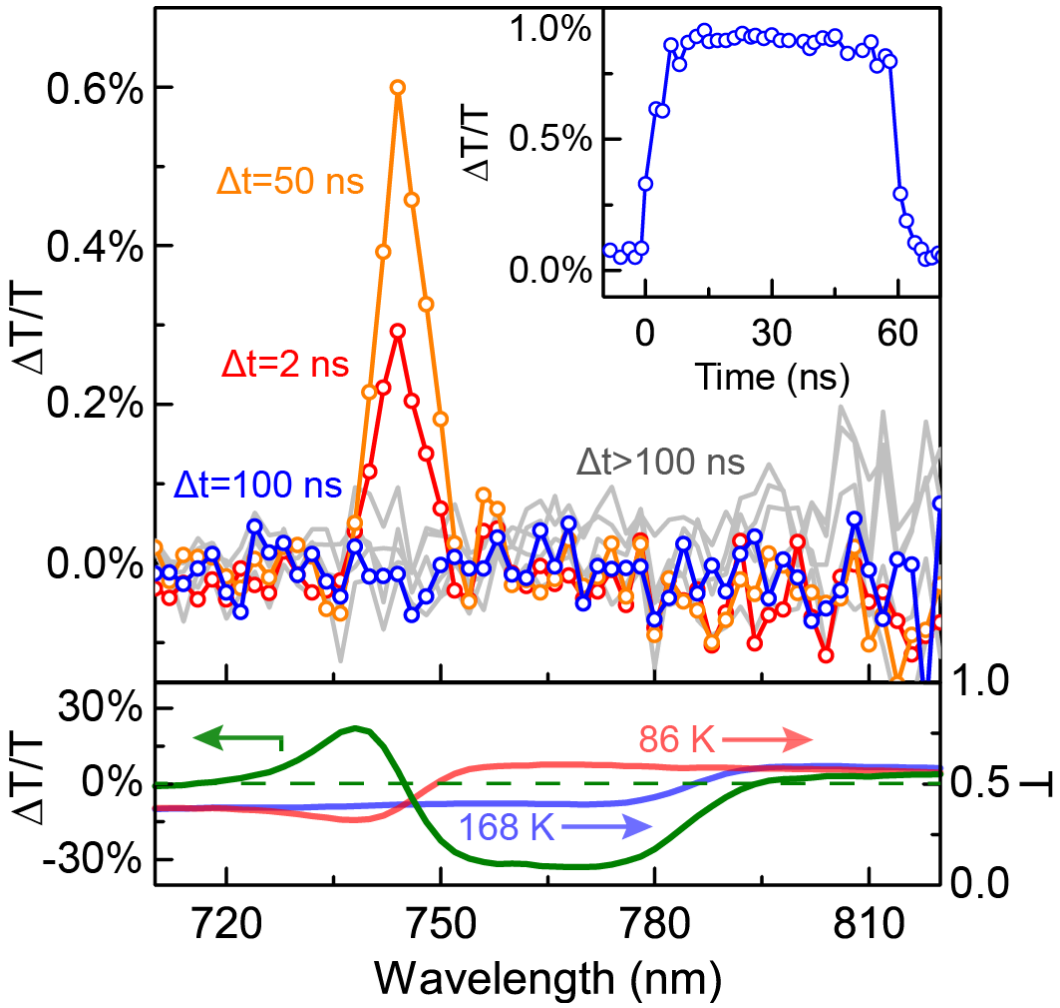

Figure 4 | Pump-induced $MAPbI_3$ phase evolution. Transient absorption (TA) spectra recorded for a $MAPbI_3$ DFB laser using super-continuum probe pulses at different times (Δt) following pump turn-on under similar conditions as in Fig. 1b; here the pump intensity is $I_P = 37.5$ kW/cm^2 and the substrate temperature is $T = 86$ K. The early time spectra display a stimulated emission bleach of the orthorhombic phase band edge that extinguishes within ~60 ns, as evident from the inset transient recorded at the peak bleach wavelength, $\lambda = 745$ nm. The magnitude of the inset transient differs slightly from the spectra because the two data sets were collected on different days on different sample cooling cycles. Notably, the spectra at longer times ($\Delta t > 100$ ns shown in gray) show no evidence of emerging tetragonal phase absorption

that would be reflected by a negative TA signal (green line) arising from the difference between the steady-state tetragonal ($T = 168$ K, light blue line) and orthorhombic ($T = 86$ K, light red line) phase transmission spectra shown in the lower panel.